ARTICLE

Reactions of Group V Metal Atoms with Hydrogen Sulfide: Argon Matrix Infrared Spectra and Theoretical Calculations†

Jie Zhao, Bing Xu, Wen-jie Yu, Xue-feng Wang*

Shanghai Key Lab of Chemical Assessment and Sustainability, Department of Chemistry, Tongji University, Shanghai 200092, China

(Dated: Received on November 16, 2015; Accepted on December 30, 2015)

The reaction of laser-ablated vanadium, niobium and tantalum atoms with hydrogen sulfide has been investigated using matrix isolation FTIR and theoretical calculations. The metal atoms inserted into the H−S bond of H_2S to form the HMSH molecules (M=V, Nb, Ta), which rearranged to H_2MS molecules on annealing for Nb and Ta. The HMSH molecule can also further react with another H_2S to form the $H_2M(SH)_2$ molecules. These new molecules were identified on the basis of the D_2S and $H_2{}^{34}S$ isotopic substitutions. DFT (B3LYP and BPW91) theoretical calculations are used to predict energies, geometries, and vibrational frequencies for these novel metal dihydrido complexes and molecules. Reaction mechanism for formation of group V dihydrido complex was investigated by DFT internal reaction coordinate calculations. The dissociation of HVSH gave VS+H_2 on broad band irradiation and reverse reaction happened on annealing. Based on B3LYP calculation releasing hydrogen from HVSH is endothermic only by 13.5 kcal/mol with lower energy barrier of 16.9 kcal/mol.

Key words: Hydrogen sulfide, Matrix isolation, Transition metal, Density functional calculation

I. INTRODUCTION

Abundant but toxic H_2S from industry and nature is a potentially valuable chemical to produce clean hydrogen energy [1]. However, it is a challenge to develop a sustainable and economical approach that can split H_2S to H_2 and S simultaneously. The splitting reaction is thermodynamically unfavorable, which needs the standard Gibbs free energy change $\Delta G^{\ominus}$ of 33 kJ/mol [2]. Up to now experiments have been done extensively for H_2S activation [3–19], and the decomposition of H_2S with photo catalysis has been explored [12, 20, 21]. Hydrogen sulfide also plays important roles in physiological processes such as vaso regulation and neutro transmission; for example, H_2S molecule is an important signaling molecule that regulates the intracellular redox status and fundamental signaling processes at physiological levels [22].

The oxidation of H_2S by transition metals has been studied both experimentally and theoretically [23–28]. Recent matrix isolation FTIR and theoretical study of reactions of laser-ablated thorium and uranium atom with H_2S in excess noble gas matrixes has been reported [29]. In solid argon group IV metal atoms insert into the S−H bond of hydrogen sulfide to form the HMSH, H_2MS, and $H_2M(SH)_2$ (M=Ti, Zr, Hf) molecules [30]. In the case of group XII metal reactions only insertion products HMSH (M=Zn, Cd, Hg) were identified. The HZnSH and HCdSH were obtained on sample annealing; however, the HHgSH was observed on UV irradiation [31].

In this work, we report here the identification of group V metal dihydrido complexes that are produced through laser-ablated V, Nb, Ta atom reactions with H_2S in solid argon. The vibration frequencies are confirmed by isotopic substitution and DFT frequency calculations. The metal dihydrido complexes observed in our experiment are instructive for designing the reversible hydrogen storage materials.

II. EXPERIMENTAL AND COMPUTATIONAL METHODS

Our experimental method has been described in detail previously [32–34]. Briefly, a Nd:YAG laser fundamental (1064 nm, 10 Hz repetition rate with 10 ns pulse width) was focused onto a rotating transition metal target through a hole in a CsI window cooled normally to 4 K by means of a closed-cycle helium refrigerator. The laser-evaporated metal atom was co-deposited with hydrogen sulfide in excess argon onto the CsI window for 1 h at a rate of 2−4 mmol/h. The H_2S, $H_2{}^{34}S$, and D_2S samples were prepared by previously described method [30]. After deposition infrared spectra were recorded

†Part of the special issue for "the Chinese Chemical Society's 14th National Chemical Dynamics Symposium".

*Author to whom correspondence should be addressed. E-mail: xfwang@tongji.edu.cn

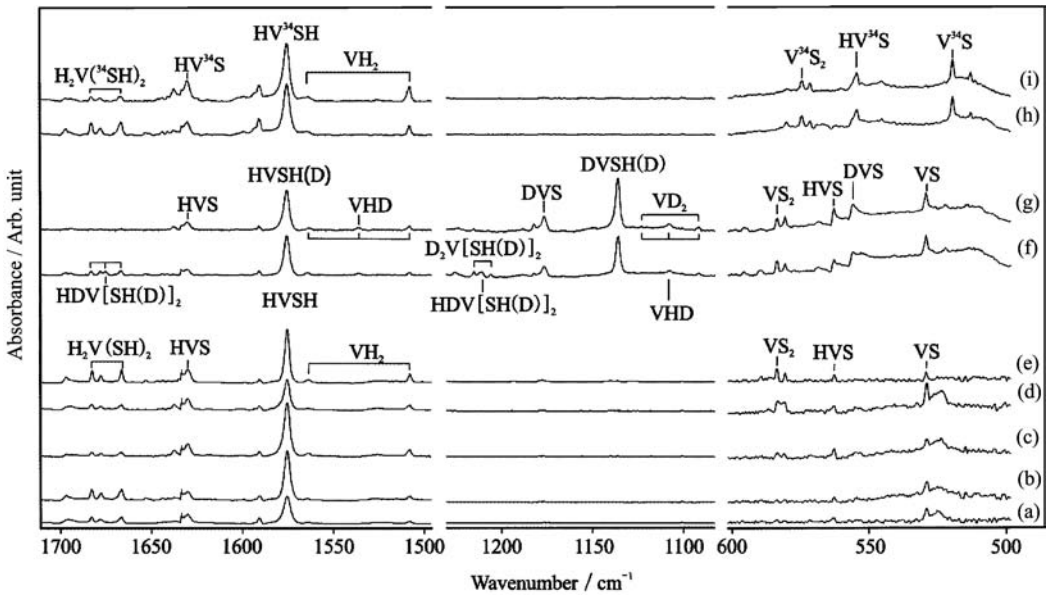

FIG. 1 Infrared spectra from the laser-ablated V atom reactions with H_2S in excess argon. (a) V+0.5%H_2S in argon codeposited for 1 h, (b) after annealing to 25 K, (c) after 300−740 nm irradiation, (d) after broad band irradiation, (e) after annealing to 30 K, (f) the laser ablated V atom reactions with 0.2%H_2S+0.2%D_2S in excess argon, after annealing to 25 K, (g) after 340−740 nm irradiation, (h) the laser ablated V atom reactions with 0.5%$H_2{}^{34}S$ in excess argon, after annealing to 25 K, (i) after 300−740 nm irradiation.

on a Bruker 80 V spectrometer at a 0.5 cm^{-1} resolution between 4000 and 400 cm^{-1} using a liquid nitrogen cooled broad band MCT detector. Matrix samples were annealed at different temperatures and were irradiated for 10 min by a mercury arc lamp (175 W) with globe removed to allow reagent diffusion and further reaction.

Quantum chemical calculations were performed using Gaussian 09 program soft package to help the assignment of vibrational frequencies of the observed reaction products [35]. The B3LYP [36] and BPW91 [37] density functional were applied and aug-cc-pVTZ-PP basis sets of Peterson *et al.*, which incorporate a relativistic pseudo potential that account for scalar relativistic effects, were employed for Nb and Ta atoms [38, 39]. The aug-cc-pVTZ basis sets were employed for V, S, and H atoms [40, 41]. The geometries of various reactants, intermediates, and products were fully optimized. The vibrational frequencies were calculated with analytic second derivatives, and zero-point energies were derived. The intrinsic reaction coordinate (IRC) calculations were carried out to ensure the obtained TSs connecting the desired reactants and products.

III. RESULTS AND DISCUSSION

A. Infrared spectra

Infrared spectra for the reactions of laser-ablated V, Nb, and Ta atoms with H_2S in excess argon in the selected regions are illustrated in Fig.1−Fig.3, and the product absorptions are listed in Table I. In V−H stretching region absorptions were observed at 1682.8, 1666.7, 1630.3, and 1575.6 cm^{-1} in experiment of vanadium atom reaction with H_2S. The deuterium counterparts appeared at 1215.4, 1206.0, 1176.9, and 1136.1 cm^{-1} in V+D_2S experiment. In addition in V−S stretching region 583.5, 562.9, and 529.4 cm^{-1} bands appeared on 300−740 nm irradiation and enhanced greatly on broad band photolysis. The 583.5 cm^{-1} band has been assigned to VS_2 molecule [43]. Reactions of Nb atoms with H_2S in excess argon produced new bands at 1726.9, 1709.8, 1695.6, and 1682.6 cm^{-1} in Nb−H stretching region and 603.1 cm^{-1} in Nb−S stretching region. Similarly Ta atom reactions in solid argon with H_2S gave new absorptions at 1796.4, 1780.7, 1785.3, 1769.4, and 649.7 cm^{-1}. For all three laser-ablated metal reactions experiments were also done with sulfur-34 isotopic-labeled samples ($H_2{}^{34}S$) and deuterium labeled samples (H_2S+HDS+D_2S), and the representative spectra in selected region are shown in Fig.1−Fig.3, respectively.

B. Calculations

Calculations at the B3LYP level of theory were done for three isomers of MH_2S, namely, the inserted HMSH and H_2MS molecules, and the $M(SH_2)$ complexes. The calculated geometric parameters and relative stabilities of HMSH and H_2MS isomers are shown in Fig.4, and the calculated vibrational frequencies and intensities are listed in Tables II−IV for observed molecules. We find the HVSH molecule is the lowest in energy for all three

DOI:10.1063/1674-0068/29/cjcp1511233

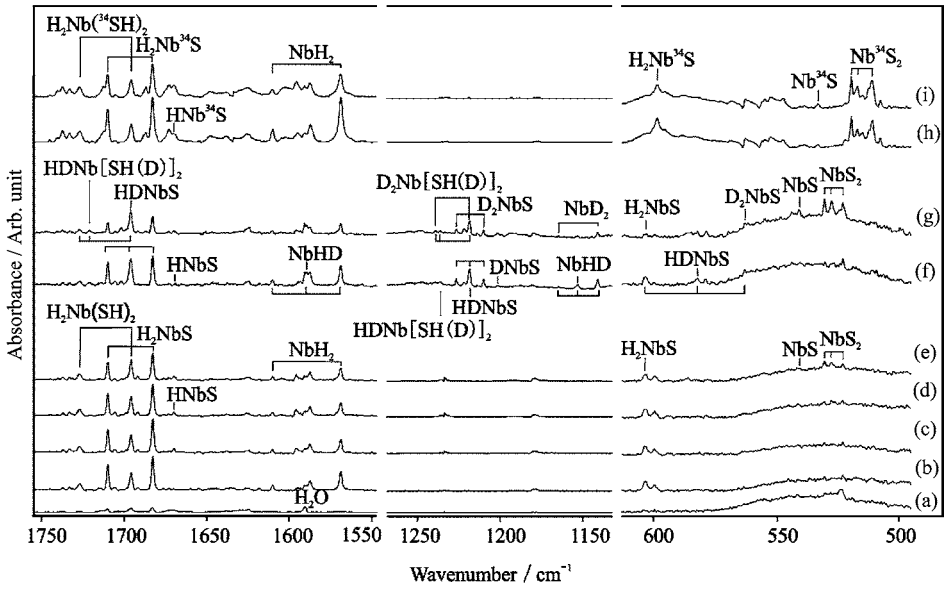

FIG. 2 Infrared spectra from the laser-ablated Nb atom reactions with H_2S in excess argon; (a) Nb+0.5%H_2S in argon code posited for 1 h, (b) after annealing to 30 K, (c) after 300−740 nm irradiation, (d) after broad band irradiation, (e) after annealing to 30 K, (f) the laser ablated Nb atom reactions with 0.2%H_2S+0.2%D_2S in excess argon, after annealing to 25 K, (g) after full-arc photolysis, (h) the laser ablated Nb atom reactions with 0.5%$H_2{}^{34}S$ in excess argon, after annealing to 25 K, (i) after broad band irradiation.

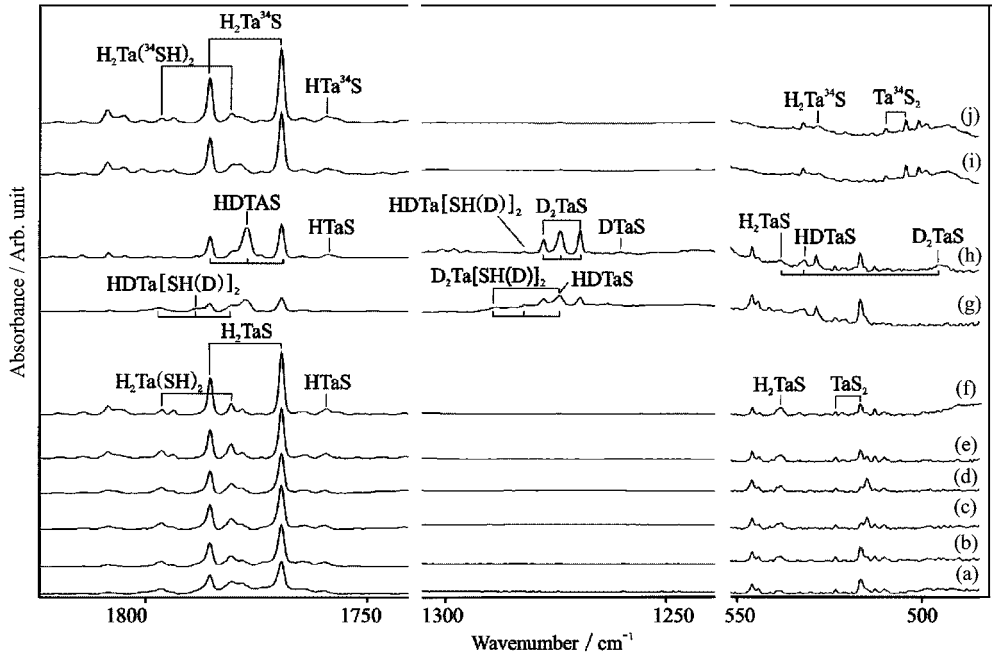

FIG. 3 Infrared spectra from the laser-ablated Ta atom reactions with H_2S in excess argon. (a) V+0.5%H_2S in argon codeposited for 1 h, (b) after annealing to 25 K (c) after 300−740 nm irradiation, (d) after broad band irradiation, (e) after annealing to 30 K, (f) the laser ablated Ta atom reactions with 0.2%H_2S+0.2%D_2S in excess argon codeposited for 1 h, (g) after annealing to 25 K, (h) the laser ablated Ta atom reactions with 0.5%$H_2{}^{34}S$ in excess argon, codeposited for 1 h, (i) after annealing to 25 K.

DOI:10.1063/1674-0068/29/cjcp1511233

TABLE I Infrared absorptions (cm^{-1}) observed for products of the reaction of V, Nb, and Ta atoms with H_2S molecules in argon.

H_2S	D_2S	$H_2{}^{34}S$	Assignment
		V+H_2S/Ar	
1682.8	1215.4	1682.8	$H_2V(SH)_2$, VH sym str
1666.7	1206.0	1666.6	$H_2V(SH)_2$, VH antisym str
1630.3	1176.9	1630.3	HVS, VH str
1575.6	1136.1	1575.6	HVSH, VH str
583.5	583.5	574.9	VS_2, VS str
562.9	556.1	554.5	HVS, VS str
529.4	529.4	519.7	VS, VS str
		Nb+H_2S/Ar	
1726.9	1249.1	1726.9	$H_2Nb(SH)_2$, NbH sym str
1709.8	1226.7	1682.8	H_2NbS, NbH sym str
1695.6	1218.8	1696.3	$H_2Nb(SH)_2$, NbH antisym str
1682.8	1210.1	1709.8	H_2NbS, NbH antisym str
1669.8	1198.8	1669.8	HNbS, NbHstr
603.4	563.3	598.3	H_2NbS, H_2NbS deform
541.2	541.2	533.9	NbS_2, NbS str
531.1	531.1	520.4	NbS_2, NbS str
		Ta+H_2S/Ar	
1796.4	1288.7	1796.4	$H_2Ta(SH)_2$, TaH sym str
1785.5	1277.6	1785.5	H_2TaS, TaHsym str
1780.7	1297.9	1780.7	$H_2Ta(SH)_2$, TaH antisym str
1769.4	1269.4	1769.4	H_2TaS, TaH antisymstr
1759.0	1260.5	1759.0	HTaS, TaH str
538.3	495.6	528.5	H_2TaS, TaS str
523.6	523.6	509.7	TaS_2, TaS str
516.6	516.6	504.3	TaS_2, TaS str

isomers; however, for Nb and Ta the dihydrido complex H_2MS are the most stable on potential energy surface as shown in Fig.5. The HMSH and H_2MS could react with H_2S to give $H_2M(SH)_2$, which were calculated also to be dihydrido complex as shown in Fig.4.

C. Vanadium

1. HVSH

Laser-ablated vanadium atom reactions with H_2S in excess argon gave the strongest new band at 1575.6 cm^{-1}, which appeared on deposition and increased on 25 K annealing, but greatly decreased on broad-band photolysis. This band showed no sulfur-34 shift, but shifted to 1136.1 cm^{-1} with D_2S, giving an isotopic H/D ratio of 1.3868, suggesting that the 1575.6 cm^{-1} band is due to V−H stretching mode. In the experiment with H_2S+HDS+D_2S mixture the doublet hydrogen isotopic distribution pattern (1575.6 and 1136.1 cm^{-1}) was observed, confirming one hydrogen atom involved in this mode. So 1575.6 cm^{-1} band is appropriate for the V−H stretching mode of HVSH molecule. Notice the V−H stretching frequency was observed for HV(OH) at 1567.0 cm^{-1} in the vanadium atom reaction with H_2O [42].

Theoretical calculations at B3LYP and BPW91 level predicted that the HVSH molecule with high-spin quartet ground state is in the global minimum energy (Fig.4). Our frequency calculation gave strong V−H stretching frequency at 1643.4 cm^{-1} (B3LYP) and 1629.6 cm^{-1} (BPW91), which is overestimated by 5.6% (B3LYP) and 3.4% (BPW91), respectively, in very good agreement with harmonic DFT frequency calculation for group V metal hydrides. In addition the calculated intensity of S−H stretching mode for HVSH is extremely weak (Table II), which is in agreement with our experiment in which this mode was not observed.

2. $H_2V(SH)_2$

Two weak bands at 1682.8 and 1666.7 cm^{-1} appeared on initial deposition of vanadium atoms with H_2S in excess argon, which increased upon annealing, but decreased on irradiation. These bands exhibited no sulfur-34 shift but shifted to 1215.4 and 1206.0 cm^{-1} with deuterium substitution, giving H/D ratio of 1.3842 and 1.3833, respectively. The isotopic H/D ratios indicate that these two bands are due to V−H stretching vibrations. Experiment with H_2S+HDS+D_2S gave triplet distribution at 1682.8, 1675.3, and 1666.6 cm^{-1} in upper V−H stretching region and 1215.4, 1211.1, and 1206.0 cm^{-1} in lower V−D stretching region, suggesting two hydrogen atoms involved in the vibrations. These bands are assigned to V−H antisymmetric and symmetric modes of isolated $H_2V(SH)_2$ molecule.

DFT frequency calculations substantiate the assignment of $H_2V(SH)_2$ molecule. Firstly, with B3LYP functional the V−H stretching modes are computed for $H_2V(SH)_2$ at 1809.1 and 1801.6 cm^{-1}, respectively, which are overestimated by about 7%. These calculated results are in line with calculated and observed frequencies for other vanadium dihydrides [45]. Secondly the calculated antisymmetric and symmetric V−H modes for $H_2V(SH)_2$ are about 160 cm^{-1} higher than the same modes for HVSH, which are in agreement with our observation. Thirdly, since the total energy of HVSH is 11 kcal/mol lower than that of H_2VS that was not observed; however, in our experiment the major product HVSH further reacts with H_2S to form $H_2V(SH)_2$ and this reaction is exothermic by 22 kcal/mol based on our B3LYP calculation. In addition our BPW91 frequency calculations as listed in Table II also support the assignment.

3. HVS

In V+H_2S experiment a V−H stretching band at 1630.3 cm^{-1} was observed on deposition and increased

DOI:10.1063/1674-0068/29/cjcp1511233

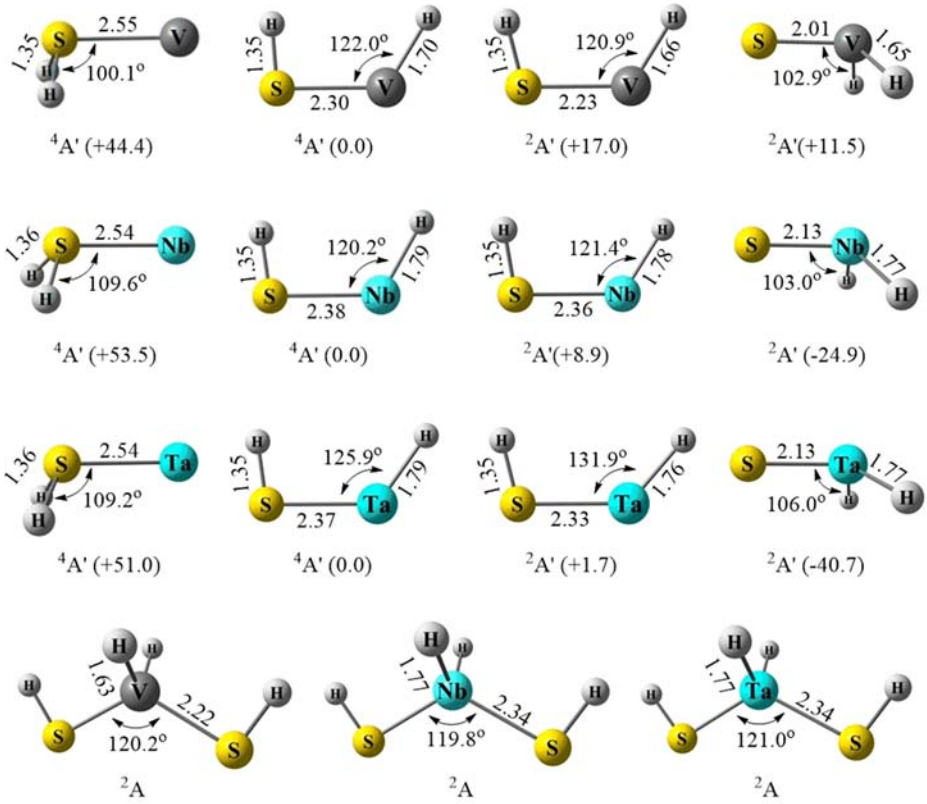

FIG. 4 B3LYP calculated geometric parameters (bond length in Å) and relative stability (kcal/mol, in parentheses) of the MH_2S (M=V, Nb, Ta) isomers and $H_2M(SH)_2$ (M=V, Nb, Ta) molecules.

slightly on 300−740 nm irradiation. This band shows no shift with $H_2{}^{34}S$ sample but moved to 1176.9 cm^{-1} with D_2S sample, giving H/D isotopic ratio of 1.3852. A weak band at 562.9 cm^{-1} tracked with 1630.3 cm^{-1} in the whole reaction process. $H_2{}^{34}S$ and D_2S, the counterpart bands, appeared at 556.1 and 554.7 cm^{-1}, defining $^{32}S/^{34}S$ and H/D ratio of 1.0122 and 1.0148, respectively. The large ^{34}S shift indicates this absorption arises mostly from the V−S stretching vibration perturbed by VH vibrations. A new triatomic HVS molecule is proposed and confirmed by DFT calculations. With B3LYP functional frequency calculation the M−H stretching mode of the HVS molecules was calculated at 1719.8 cm^{-1}, which is overestimated by 5.5%. In addition M−S stretching modes was predicted at 577.8 cm^{-1} that is in very good agreement with observation.

4. VS and VS_2

In the V+H_2S experiment a weak band in V−S stretching region at 529.4 cm^{-1} is due to diatomic VS molecule, which was observed on deposition and greatly enhanced on broad band photolysis at the expense of HVSH and $H_2V(SH)_2$ molecules. This band exhibited no deuterium isotopic shift but shifted to 519.7 cm^{-1} with $H_2{}^{34}S$, and gave an isotopic $^{32}S/^{34}S$ ratio of 1.0187. H_2S+$H_2{}^{34}S$ mixture (not shown) doublet distribution at 529.4 and519.7 cm^{-1} was observed and assignment of VS is confirmed. Notice this band was observed weakly in early vanadium atom reaction with discharged sulfur vapor [43]. Another band at 583.5 cm^{-1} appeared on 300−740 nm irradiation and enhanced greatly on broad-band photolysis, which has been assigned to VS_2 molecule [43]. The V−S stretching modes for VS and VS_2 molecules were calculated at 539.8 and 593.0 cm^{-1} (B3LYP), respectively, which are overestimated by only 10 cm^{-1}. The calculated BPW91 frequencies are even better matching observed values (Table II).

D. Niobium

1. H_2NbS and $H_2Nb(SH)_2$

The absorptions at 1709.8, 1682.8 and 603.4 cm^{-1} in the Nb+H_2S experiments are assigned to the H_2NbS molecule. These three bands increased on annealing and decreased on broad-band irradiation. The 1709.8 and 1682.8 cm^{-1} bands show no sulfur-34 shift with $H_2{}^{34}S$ sample, but with deuterium enriched sample these bands shift to 1226.7 and 1210.1 cm^{-1}, defying H/D ratios of 1.3938 and 1.3906, respectively, which are typical Nb−H stretching vibrations. In the mixed H_2S+HDS+D_2S experiments, two intermediate bands

DOI:10.1063/1674-0068/29/cjcp1511233

TABLE II Calculated frequencies for HVSH, H_2VS, $H_2V(SH)_2$, HVS, VS, and VS_2.

	H_2S		D_2S		$H_2{}^{34}S$		Description
	B3LYP	BPW91	B3LYP	BPW91	B3LYP	BPW91	
HVSH	2661.1(2)	2603.6(4)	1910.5(2)	1869.3(3)	2658.7(2)	2601.3(4)	S−H str
	1643.4(343)	1629.6(264)	1174.1(180)	1164.2(138)	1643.4(343)	1629.6(264)	V−H str
	465.2(44)	459.8(70)	337.9(9)	398.2(66)	464.9(44)	459.4(68)	VH-SH wagging
	397.4(134)	400.9(64)	387.6(88)	331.0(11)	391.9(139)	394.9(68)	V−SH str
	321.5(55)	318.0(48)	235.7(50)	230.9(36)	320.0(50)	316.9(45)	HVSH scissoring
	207.8(90)	217.3(70)	150.5(50)	157.2(39)	207.6(89)	217.1(70)	HVSH rocking
H_2VS	1789.9(222)	1752.8(153)	1275.0(117)	1248.5(81)	1789.9(222)	1752.8(153)	V−H sym str
	1772.4(268)	1738.1(222)	1271.5(141)	1246.8(116)	1772.4(268)	1738.1(222)	V−H antisym str
	665.0(136)	648.9(126)	622.3(79)	608(66)	660.5(136)	644.4(127)	H_2VS deform
	565.4(43)	557.6(57)	429.4(34)	420.5(41)	559.4(44)	552.4(58)	VH_2 scissoring
	451.1(103)	469.3(75)	330.2(60)	344.7(47)	450.4(102)	468.6(36)	VH_2 bending
	445.5(33)	469.0(36)	323.4(14)	339.9(16)	445.1(33)	468.1(71)	VH_2 rocking
$H_2V(SH)_2$	2614.8(0)	2540.2(0)	1877.1(0)	1823.7(0)	2612.5(0)	2537.9(0)	S−H str
	2614.6(9)	2539.6(3)	1876.9(5)	1823.2(2)	2612.3(9)	2537.4(3)	S−H str
	1809.1(149)	1749.6(117)	1293.1(104)	1253.6(90)	1809.1(149)	1749.6(117)	V−H sym str
	1801.6(201)	1746.0(174)	1288.2(80)	1245.2(62)	1801.6(201)	1746.0(174)	V−H antisym str
	626.6(79)	634.8(67)	471.5(25)	476.5(24)	626.5(78)	634.6(67)	VH_2 deform
	584.7(95)	566.3(69)	514.8(114)	503.6(77)	582.6(91)	564.0(66)	VH_2 bending
HVS	1719.8(256)	1708.3(186)	1229.2(134)	1220.8(96)	1719.8(256)	1708.3(186)	V−H str
	577.8(103)	624.6(90)	569.9(67)	617.7(60)	568.8(105)	614.7(92)	V−S str
	452.0(64)	474.9(78)	332.1(41)	347.2(46)	450.4(61)	473.5(75)	V−H bending
VS	539.8(66)	538.7(40)			530.0(64)	528.9(39)	V−S str
VS_2	593.0(130)	582.3(105)			583.7(127)	573.0(102)	V−S str
	542.8(7)	540.9(7)			531.8(6)	530.2(7)	V−S antisym str
	165.4(1)	176.9(0)			161.6(0)	172.8(0)	VS_2 scissoring

were observed at 1696.1 and 1218.6 cm^{-1}; which clearly show that two equivalent H atoms are involved in this molecule. The 603.4 cm^{-1} band shifted to 598.3 cm^{-1} with $H_2{}^{34}S$ and to 563.3 cm^{-1} with D_2S, giving $^{32}S/^{34}S$ ratio of 1.0085 and H/D ratio of 1.0711, respectively. An intermediate band at 582.2 cm^{-1} appeared in the mixed H_2S+HDS+D_2S experiments. Accordingly, the 1709.8 and 1682.8 cm^{-1} bands are assigned to the Nb−H symmetry and anti-symmetry stretching vibrations and the 603.4 cm^{-1} band is assigned to NbH_2 bending vibration coupled with the NbS vibration in H_2NbS molecule.

In the reactions of atomic Nb with H_2S in solid argon, absorptions at 1726.9 and 1695.6 cm^{-1} track together, which are located in Nb−H stretching region. These bands are weak on initial deposition and increasing greatly on annealing to 25 K and further increasing by 50% on annealing to 30 K. With $H_2{}^{34}S$ there were no shifts observed but with deuterium substitution two bands shifted to 1249.2 and 1218.8 cm^{-1}, defining 1.3824 and 1.3912 H/D ratios, respectively. In the mixture H/D isotopic experiment (H_2S+HDS+D_2S) two triplets were observed in upper Nb−H and lower Nb−D stretching regions. These bands favored on later annealing, suggesting the product comes from niobium atom reaction with more H_2S molecules. Accordingly the $H_2Nb(SH)_2$ molecule is proposed.

The B3LYP calculation predicted that the H_2NbS has a $^2A'$ ground state and NbH symmetric and antisymmetric stretching modes are calculated at 1787.3 and 1772.6 cm^{-1}, which are overestimated by 4.5% and 5.3%, respectively. The predicted H-Nb−S bending mode at 679.1 cm^{-1} shows 2 cm^{-1} shift with S-34 substitution and 97 cm^{-1} shift with deuterium substitution, which match the observed values very well. Our BPW91 frequency computation predicted the Nb−H symmetric and antisymmetric stretching modes of $H_2Nb(SH)_2$ at 1761.6 and 1750.3 cm^{-1}, which are overestimated by 3.0% and 4.0%, respectively.

2. NbS and NbS_2

In the Nb+H_2S experiments, a weak band at 541.2 cm^{-1} observed on deposition increased 50% on 300−700 nm irradiation. This band showed no deuterium shift but shifted to 533.9 cm^{-1} with $H_2{}^{34}S$ sample, giving 1.0137 isotopic ratio, which is appropriate for diatomic NbS molecule. A band at 531.1 cm^{-1}

DOI:10.1063/1674-0068/29/cjcp1511233

TABLE III Calculated frequencies for HNbSH, H_2NbS, $H_2Nb(SH)_2$, HNbS, NbS, and NbS_2.

	H_2S		D_2S		$H_2{}^{34}S$		Description
	B3LYP	BPW91	B3LYP	BPW91	B3LYP	BPW91	
HNbSH	2652.4(4)	2590.7(3)	1904.5(3)	1860.4(2)	2650.0(4)	2588.4(3)	S−H str
	1701.7(305)	1691.9(236)	1210.4(156)	1203.4(120)	1701.7(305)	1691.9(236)	Nb−H str
	501.4(36)	487.8(47)	357.5(1)	385.3(49)	501.0(36)	487.3(46)	NbH-SH wagging
	385.7(97)	384.2(54)	379.4(66)	344.4(3)	380.1(101)	378.0(58)	Nb−SH str
	330.9(24)	331.4(26)	243.0(32)	241.1(26)	328.3(18)	329.4(22)	HNbSH scissoring
	199.0(55)	204(47)	143.9(30)	147.4(25)	198.8(55)	208(47)	HNbSH rocking
H_2NbS	1787.3(204)	1761.6(150)	1268.6(105)	1250.4(77)	1787.3(204)	1761.6(150)	Nb−H sym str
	1772.6(332)	1750.3(274)	1264.1(171)	1248.2(141)	1772.6(332)	1750.3(274)	Nb−H antisym str
	679.1(109)	672.6(92)	582.2(77)	570.6(59)	677.8(107)	671.8(91)	H_2NbS deform
	562.4(72)	561.7(72)	462.6(33)	464.1(34)	552.2(75)	552.1(76)	Nb−S str
	487.8(23)	491.6(26	353.1(10)	355.4(12)	487.3(23)	491.2(27)	NbH_2 rocking
	450.7(62)	463.0(40)	328.5(41)	339.3(31)	449.4(59)	461.0(36)	NbH_2 bending
$H_2Nb(SH)_2$	2578.1(0)	2502.7(1)	1850.8(0)	1796.7(0)	2575.8(0)	2600.5(1)	S−H str
	2577.2(0)	2499.5(4)	1850.0(0)	1794.4(2)	2574.9(0)	2497.3(4)	S−H str
	1801.3(158)	1760.0(127)	1278.5(82)	1249.0(65)	1801.3(158)	1760.0(127)	Nb−H sym str
	1786.4(267)	1749.9(226)	1274.0(137)	1248.1(116)	1786.4(267)	1750.0(225)	Nb−H antisym str
	622.5(72)	640.6(54)	462.9(17)	470.7(17)	622.3(72)	640.5(54)	NbH_2 scissoring
	540.1(90)	524.1(65)	451.6(97)	445.1(66)	538.7(87)	522.3(63)	NbH_2 bending
HNbS	1759.3(223)	1790.4(146)	1251.6(114)	1273.5(74)	1759.3(223)	1790.4(146)	Nb−H str
	568.0(96)	579.5(51)	558.4(65)	569.4(36)	557.9(98)	570.4(52)	Nb−S str
	474.9(24)	521.1(9)	348.2(21)	382.0(10)	472.5(21)	517.4(7)	Nb−H bending
NbS	543.9(47)	535.1(32)			531.9(45)	523.3(30)	Nb−S str
NbS_2	542.3(14)	533.2(10)			529.7(13)	520.8(9)	Nb−S str
	539.5(116)	531.3(89)			528.4(113)	520.4(86)	Nb−S antisym str
	177.6(0)	179.6(0)			173.3(0)	175.3(0)	NbS_2 scissoring

appeared on co-deposition and increased on broad-band photolysis, and shifted to 520.4 cm^{-1} with $H_2{}^{34}S$ sample, defining the $^{32}S/^{34}S$ isotopic ratio of 1.0206. This band has been assigned to NbS_2 molecule [43]. The NbS stretching mode is predicted at 539.4 cm^{-1}, which is overestimated by 1.5%. Notice the increase of 541.2 cm^{-1} band is at expense of H_2NbS on UV irradiation.

E. Tantalum

1. H_2TaS and $H_2Ta(SH)_2$

In solid argon, the reactions of Ta with H_2S gave a set of bands at 1785.5, 1769.4 and 538.3 cm^{-1}, which tracked together in the whole reaction process. These bands appeared on the co-deposition, increased two folds on 25 K annealing, slightly increased on 300−740 nm irradiation, but decreased on broad band irradiation. The 1785.5 and 1769.4 cm^{-1} bands showed no ^{34}S shift but moved to 1277.6 and 1269.4 cm^{-1} with D_2S sample, defining the 1.3975 and 1.3935 H/D ratios. The 538.3 cm^{-1} band shifted to 528.5 cm^{-1} with $H_2{}^{34}S$ defining the isotopic $^{32}S/^{34}S$ ratio of 1.0187, and the deuterium counterpart was observed at 495.6 cm^{-1}, giving H/D ratio of 1.0862. Using a mixed H_2S+HDS+D_2S sample, three triplet band distributions were observed in upper Ta−H stretching region at 1785.5, 1777.1, and 1769.4 cm^{-1}, lower Ta−D stretching region at 1277.6, 1274.0, and 1269.4 cm^{-1}, and Ta-S stretching region at 538.3, 531.7 and 495.6 cm^{-1}, indicating two H atoms are involved in the molecule. On the basis of the above spectroscopic information, this set of bands is assigned to the H_2TaS molecule. Notice the 1777.1, 1274.0 and 531.7 cm^{-1} bands are due to Ta−H and Ta−D stretching, and TaHD bending vibrations of HDTaS, respectively.

The 1796.4 and 1780.7 cm^{-1} absorptions in the Ta+H_2S experiments are assigned to $H_2Ta(SH)_2$ molecule. Two bands increased on annealing to 25 K, slightly decreased on full-arc photolysis and increased again on annealing to 30 K. These two bands showed no sulfur-34 shift with $H_2{}^{34}S$ sample and the deuterium counterparts were found at 1288.7 and 1277.6 cm^{-1}, giving 1.3940 and 1.3938 H/D ratios. Two triplet distributions appeared in upper Ta−H and lower Ta−D stretching regions in the mixed H_2S+HDS+D_2S experiments, indicating two equivalent H atoms included in

DOI:10.1063/1674-0068/29/cjcp1511233

TABLE IV Calculated frequencies for HNbSH, H_2NbS, $H_2Nb(SH)_2$, HNbS, NbS, and NbS_2.

	H_2S		D_2S		$H_2{}^{34}S$		Description
	B3LYP	BPW91	B3LYP	BPW91	B3LYP	BPW91	
HTaSH	2651.4(5)	2591.4(4)	1903.8(3)	1860.9(2)	2649.0(5)	2589.0(4)	S−H str
	1779.4(243)	1764.9(198)	1262.3(123)	1252.1(100)	1779.4(243)	1764.9(198)	Ta−H str
	523.9(12)	507.8(21)	379.0(16)	377.6(33)	523.5(12)	507.3(21)	TaH−SH wagging
	390.8(71)	387.9(49)	364.6(29)	355.4(2)	386.2(71)	383.1(50)	Ta−SH str
	326.2(2)	330.4(3)	247.6(12)	248.4(12)	321.7(1)	326.0(2)	HTaSH scissoring
	127(34)	142.9(30)	92.6(18)	103.8(16)	126.7(34)	142.7(30)	HTaSH rocking
H_2TaS	1845.7(177)	1814.4(136)	1307.7(89)	1285.6(69)	1845.7(177)	1814.4(136)	Ta−H sym str
	1829.1(282)	1800.8(242)	1299.7(143)	1279.4(123)	1829.1(282)	1800.8(242)	Ta−H antisym str
	736.2(37)	732.4(27)	568.7(53)	558.0(39)	735.6(36)	732.0(27)	H_2TaS deform
	547.0(58)	545.0(54)	497.6(10)	499.4(10)	534.9(60)	533.9(57)	Ta−S str
	498.3(12)	499.9(16)	359.8(5)	360.8(7)	497.8(12)	499.4(16)	TaH_2 rocking
	445(30)	457.0(19)	322.5(21)	333.1(17)	444.1(27)	454.7(15)	TaH_2 bending
$H_2Ta(SH)_2$	2550.6(1)	2469.3(3)	1830.9(1)	1772.5(1)	2548.4(1)	2467.2(3)	S−H str
	2548.4(5)	2462.9(25)	1829.3(2)	1768.0(13)	2546.2(5)	2460.8(25)	S−H str
	1862.2(115)	1825.3(97)	1319.7(59)	1293.5(49)	1862.2(115)	1825.3(97)	Ta−H sym str
	1844.9(245)	1810.8(211)	1310.7(124)	1286.5(107)	1844.9(245)	1810.8(211)	Ta−H antisym str
	645.8(39)	657.8(28)	470.7(9)	475.7(7)	645.6(39)	657.7(28)	TaH_2 scissoring
	545.2(79)	531.4(52)	428.6(76)	423.8(50)	544.2(76)	530.2(51)	TaH_2 bending
HTaS	1825.3(177)	1850.0(86)	1295.0(90)	1312.4(44)	1825.3(177)	1850.0(86)	Ta−H str
	553.1(70)	551.7(20)	540.8(47)	546.7(20)	542.7(71)	539.3(19)	Ta−S str
	475.2(8)	470.0(0)	349.1(12)	340.5(0)	471.7(5)	468.3(0)	Ta−H bending
TaS	527.9(31)	520.5(22)			514.5(29)	507.3(21)	Ta−S str
TaS_2	534.5(9)	523.7(6)			520.4(8)	510.0(6)	Ta−S str
	517.5(86)	508.7(67)			505.0(82)	496.4(64)	Ta−S antisym str
	170.6(0)	171.7(0)			166.2(0)	167.3(0)	TaS_2 scissoring

the molecule. Accordingly these bands were assigned to $H_2Ta(SH)_2$ molecule.

B3LYP calculation predicted that the H_2TaS molecule has a $^2A'$ ground state with nonplanar geometry. The Ta−H stretching and HTaH bending vibrations were calculated at 1845.7, 1829.1, and 547.0 cm^{-1}, respectively, which require scaling factor of 0.967, 0.967, and 0.984. The calculated Ta−H symmetric and antisymmetric stretching modes of $H_2Ta(SH)_2$ are at 1862.2 and 1844.9 cm^{-1} which match the observed values very well. Notice our BPW91 frequency calculations also support band assignments for H_2TaS and $H_2Ta(SH)_2$ molecules.

F. Other absorptions

In Nb+H_2S experiment a new Nb−H mode at 1672.7 cm^{-1} appeared on visible light irradiation and shifted to 1198.8 with D_2S sample. Similarly in the Ta+H_2S experiment a new Ta−H stretching frequency at 1759.0 cm^{-1} was observed, which shifted to 1260.5 cm^{-1}, defying 1.3955 H/D ratio. The triatomic molecule HMS (M=Zr, Hf) comes into mind for these band assignment though the M−S stretching frequencies are missing. The M−H stretching modes of the HMS molecules were calculated at 1759.3 cm^{-1} (Nb) and 1825.3 cm^{-1} (Ta) with B3LYP calculation, which are overestimated by 5.4% and 3.8%, respectively. In addition M−S stretching modes were predicted at 548.8 cm^{-1} (Nb) and 553.1 cm^{-1} (Ta). Unfortunately these modes were not observed in our experiments.

G. Reaction mechanism

As shown in Fig.5, the formations of VSH_2 ($^4A'$), $NbSH_2$ ($^4A'$), and $TaSH_2$ ($^4A'$) complexes from metal atom and hydrogen sulfide are calculated exothermically by 5.8, 13.0, and 5.2 kcal/mol, respectively. These complexes are extremely reactive, which rearrange to insertion products HMSH by hydrogen shift from sulfur atoms to metal atoms exothermically by 44.0, 53.5, and 52.5 kcal/mol for HVSH, HNbSH, and HTaSH. Next, the second hydrogen atom on sulfur atom of the insertion products can shift to metal atom to produce the dihydrido complex H_2MS.

$$M + H_2S \rightarrow MSH_2 \rightarrow HMSH \rightarrow H_2MS$$

DOI:10.1063/1674-0068/29/cjcp1511233

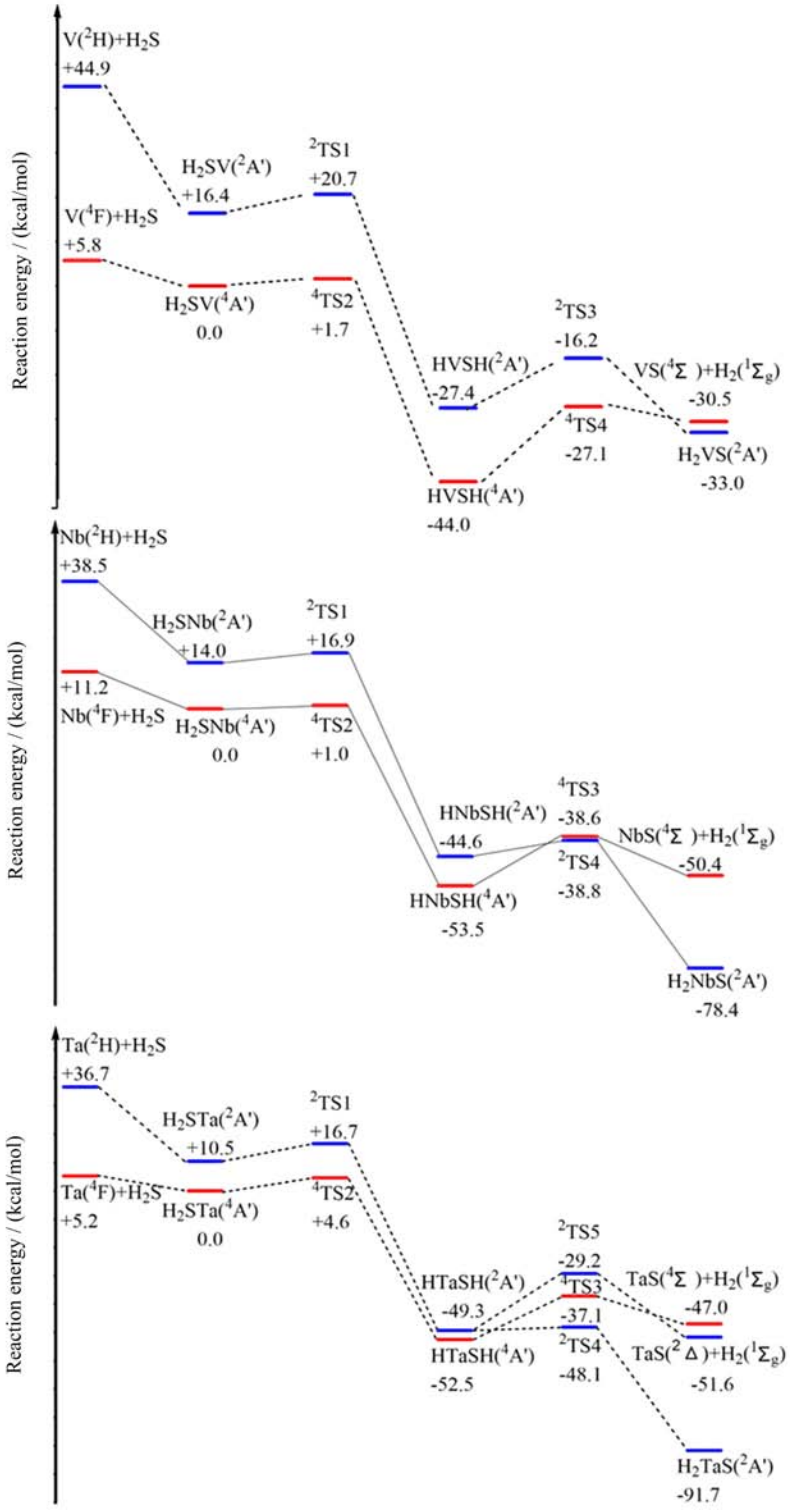

FIG. 5 Potential energy surface for reaction of V, Nb, Ta with H_2S at B3LYP level of theory.

It should be noted that the $H_2VS(^2A')$ is 11.1 kcal/mol higher in energy than HVSH, indicating the formation of HVSH is thermodynamically favored, which is in accord with our observation that main reaction product is HVSH in the experiment of V+H_2S in argon matrix. However for Nb and Ta, dihydrido complex H_2MS is more stable. $H_2NbS(^2A')$ and $H_2TaS(^2A')$ are 24.9 and 39.2 kcal/mol lower in energy than $HNbSH(^4A')$ and $HTaSH(^4A')$, respectively. In Nb and Ta reactions with H_2S, the H_2NbS and H_2TaS were observed as major

DOI:10.1063/1674-0068/29/cjcp1511233

products. Notice there is spin crossing to form these molecules from HMSH but in low temperature matrix spin crossing has high efficiency since the $^4A'$ and $^2A'$ states of HNbSH and HTaSH lies very close in energy.

The diatomic VS molecule increased on photolysis and decreased on annealing with HVSH behavior on the contrary way in V+H_2S experiment, indicating the dissociation of HVSH gave VS+H_2, and reverse reaction happened on annealing. Compared with the reaction of V with H_2O in argon matrix reported by Zhou *et al.*, where the release of hydrogen from HVOH is endothermic by about 17.3 kcal/mol with a barrier as high as 35.8 kcal/mol based on theoretical calculation [42]. However, releasing hydrogen from HVSH is endothermic only by 13.5 kcal/mol with lower energy barrier of 16.9 kcal/mol, indicating vanadium sulfides may be a better hydrogen energy storage material than vanadium oxides as the hydrogen storage and release process are easier to take place. Metal sulfides such as MoS_x and BiS_x have potential applications for hydrogen storage because of their unique characteristics of strong gas adsorptions [44].

Furthermore, the insertion products HMSH can also react with H_2S to give $H_2M(SH)_2$ on annealing.

$$\begin{aligned} HVSH(^4A') + H_2S(^1A_1) &\rightarrow H_2V(SH)_2(^2A) \\ \Delta E &= -21.6 \text{ kcal/mol} \\ HNbSH(^4A') + H_2S(^1A_1) &\rightarrow H_2Nb(SH)_2(^2A) \\ \Delta E &= -60.1 \text{ kcal/mol} \\ HTaSH(4A') + H_2S(^1A_1) &\rightarrow H_2Ta(SH)_2(^2A) \\ \Delta E &= -77.1 \text{ kcal/mol} \end{aligned}$$

The $H_2M(SH)_2$ molecules were decomposed into hydrogen and MS_2 under broad-band photolysis, which are endothermic by 16.3, 19.5, and 22.4 kcal/mol, respectively.

$$H_2M(SH)_2 \rightarrow MS_2 + H_2$$

IV. CONCLUSION

The reactions of laser-ablated V, Nb, and Ta atoms with sulfur hydride have been investigated using matrix isolation FTIR and theoretical calculations. The V, Nb, and Ta atoms inserted into the H−S bond of sulfur hydride to form the HMSH molecules (M=V, Nb, Ta), which further rearrange to H_2MS molecules on annealing for Nb and Ta. HMSH can also further react with other sulfur hydride to form the $H_2M(SH)_2$ molecules. The molecules were identified on the basis of the D_2S and $H_2{}^{34}S$ isotopic substitutions as well as density functional calculations. Qualitative analysis of the reaction paths leading to the observed products was proposed. The H_2 elimination process was observed for group V metal dihydrido complexes on broad band irradiation.

V. ACKNOWLEDGMENTS

This work was supported by the National Natural Science Foundation of China (No.21173158 and No.21373152) and the Ministry of Science and Technology of China (No.2012YQ220113-7).

[1] J. Zaman and A. Chakma, Fuel Process. Technol. **41**, 159 (1995).
[2] H. Shiina, M. Oya, K. Yamashita, A. Miyoshi, and H. Matsui, J. Phys. Chem. **100**, 2136 (1996).
[3] T. Chivers, J. B. Hyne, and C. Lau, Int. J. Hydrogen Energy **5**, 499 (1980).
[4] E. A. Fletcher, J. E. Noring, and J. P. Murray, Int. J. Hydrogen Energy **9**, 587 (1984).
[5] J. F. Reber and K. Meier, J. Phys. Chem. **88**, 5903 (1984).
[6] D. W. Kalina and E. T. Maas Jr., Int. J. Hydrogen Energy **10**, 163 (1985).
[7] D. W. Kalina and E. T. Maas Jr., Int. J. Hydrogen Energy **10**, 157 (1985).
[8] J. F. Reber and M. Rusek, J. Phys. Chem. **90**, 824 (1986).
[9] L. M. Al-Shamma and S. A. Naman, Int. J. Hydrogen Energy **15**, 1 (1990).
[10] K. Petrov and S. Srinivasan, Int. J. Hydrogen Energy **21**, 163 (1996).
[11] S. V. Tambwekar and M. Subrahmanyam, Int. J. Hydrogen Energy **22**, 959 (1997).
[12] Z. Lei, W. You, M. Liu, G. Zhou, T. Takata, M. Hara, K. Domen, and C. Li, Chem. Commun. 214 (2003).
[13] H. Wang, Int. J. Hydrogen Energy **32**, 3907 (2007).
[14] G. B. Zhao, S. John, J. J. Zhang, J. C. Hamann, S. S. Muknahallipatna, S. Legowski, J. F. Ackerman, and M. D. Argyle, Chem. Eng. Sci. **62**, 2216 (2007).
[15] H. Huang, Y. Yu, and K. H. Chung, **23**, 4420 (2009).
[16] T. Nunnally, K. Gutsol, A. Rabinovich, A. Fridman, A. Starikovsky, A. Gutsol, and R. W. Potter, Int. J. Hydrogen Energy **34**, 7618 (2009).
[17] H. Yan, J. Yang, G. Ma, G. Wu, X. Zong, Z. Lei, J. Shi, and C. Li, J. Catal. **266**, 165 (2009).
[18] E. Linga Reddy, V. M. Biju, and C. Subrahmanyam, Appl. Energy **95**, 87 (2012).
[19] X. Zong, J. Han, B. Seger, H. Chen, G. Lu, C. Li, and L. Wang, Angew. Chem. Int. Ed. **53**, 4399 (2014).
[20] G. Ma, H. Yan, X. Zong, B. Ma, H. Jiang, F. Wen, and C. Li, Chin. J. Catal. **29**, 313 (2008).
[21] G. Ma, H. Yan, J. Shi, X. Zong, Z. Lei, and C. Li, J. Catal. **260**, 134 (2008).
[22] F. Yu, X. Han, and L. Chen, Chem. Commun. **50**, 12234 (2014).
[23] A. J. Tursi and E. R. Nixon, J. Chem. Phys. **53**, 518 (1970).
[24] R. R. Smardzewski and M. C. Lin, J. Chem. Phys. **66**, 3197 (1977).
[25] E. L. Woodbridge, T. L. Tso, M. P. McGrath, W. J. Hehre, and E. K. C. Lee, J. Chem. Phys. **85**, 6991 (1986).
[26] J. D. Carpenter and B. S. Ault, J. Phys. Chem. **96**, 7913 (1992).

DOI:10.1063/1674-0068/29/cjcp1511233

[27] E. Isoniemi, M. Pettersson, L. Khriachtchev, J. Lundell, and M. Räsänen, J. Phys. Chem. A **103**, 679 (1999).
[28] S. J. Thompson, N. Goldberg, and B. S. Ault, PCCP **8**, 856 (2006).
[29] X. Wang, L. Andrews, K. S. Thanthiriwatte, and D. A. Dixon, Inorg. Chem. **52**, 10275 (2013).
[30] Q. Wang, J. Zhao, and X. Wang, J. Phys. Chem. A (2014).
[31] Z. Pan, X. Liu, J. Zhao, and X. Wang, J. Mol. Spectrosc. **310**, 16 (2015).
[32] L. Andrews, X. Wang, Y. Gong, G. P. Kushto, B. Vlaisavljevich, and L. Gagliardi, J. Phys. Chem. A **118**, 5289 (2014).
[33] L. Andrews, Chem. Soc. Rev. **33**, 123 (2004).
[34] X. Liu, X. Wang, B. Xu, and L. Andrews, PCCP **16**, 2607 (2014).
[35] M. J. Frisch, G. W. Trucks, H. B. Schlegel, G. E. Scuseria, M. A. Robb, J. R. Cheeseman, G. Scalmani, V. Barone, B. Mennucci, G. A. Petersson, H. Nakatsuji, M. Caricato, X. Li, H. P. Hratchian, A. F. Izmaylov, J. Bloino, G. Zheng, J. L. Sonnenberg, M. Hada, M. Ehara, K. Toyota, R. Fukuda, J. Hasegawa, M. Ishida, T. Nakajima, Y. Honda, O. Kitao, H. Nakai, T. Vreven, J. A. Montgomery Jr., J. E. Peralta, F. Ogliaro, M. Bearpark, J. J. Heyd, E. Brothers, K. N. Kudin, V. N. Staroverov, T. Keith, R. Kobayashi, J. Normand, K. Raghavachari, A. Rendell, J. C. Burant, S. S. Iyengar, J. Tomasi, M. Cossi, N. Rega, J. M. Millam, M. Klene, J. E. Knox, J. B. Cross, V. Bakken, C. Adamo, J. Jaramillo, R. Gomperts, R. E. Stratmann, O. Yazyev, A. J. Austin, R. Cammi, C. Pomelli, J. W. Ochterski, R. L. Martin, K. Morokuma, V. G. Zakrzewski, G. A. Voth, P. Salvador, J. J. Dannenberg, S. Dapprich, A. D. Daniels, Ö. Farkas, J. B. Foresman, J. V. Ortiz, J. Cioslowski, and D. J. Fox, *Gaussian 09, Revision C.01*, Wallingford CT: Gaussian, Inc., (2010).
[36] C. Lee, W. Yang, and R. G. Parr, Phys. Rev. B **37**, 785 (1988).
[37] J. P. Perdew and Y. Wang, Phys. Rev. B **45**, 13244 (1992).
[38] K. A. Peterson, D. Figgen, M. Dolg, and H. Stoll, J. Chem. Phys. **126**, (2007).
[39] D. Figgen, K. A. Peterson, M. Dolg, and H. Stoll, J. Chem. Phys. **130**, (2009).
[40] D. E. Woon and T. H. Dunning, J. Chem. Phys. **100**, 2975 (1994).
[41] D. E. Woon and T. H. Dunning, J. Chem. Phys. **98**, 1358 (1993).
[42] M. Zhou, J. Dong, L. Zhang, and Q. Qin, J. Am. Chem. Soc. **123**, 135 (2000).
[43] B. Liang and L. Andrews, J. Phys. Chem. A **106**, 3738 (2002).
[44] C. H. Lai, M. Y. Lu, and L. J. Chen, J. Mater. Chem. **22**, 19 (2012).
[45] X.F. Wang and L. Andrews, J. Phys. Chem. A **115**, 14175 (2002).

DOI:10.1063/1674-0068/29/cjcp1511233